AIAA JOURNAL
Vol. 60, No. 7, July 2022

Acoustic Shock Formation in Noise Propagation During Military Aircraft Ground Run-Up Operations

Brent O. Reichman,* Kent L. Gee,† Tracianne B. Neilsen,‡ and S. Hales Swift§
Brigham Young University, Provo, Utah 84602
Alan T. Wall¶
Air Force Research Laboratory, Wright–Patterson Air Force Base, Ohio 45433
and
J. Micah Downing** and Michael M. James††
Blue Ridge Research and Consulting, LLC, Asheville, North Carolina 28801

https://doi.org/10.2514/1.J060307

A distinctive feature of many high-amplitude jet noise waveforms is the presence of acoustic shocks. Metrics indicative of shock presence, specifically the skewness of the time derivative of the waveform, the average steepening factor, and a new wavelet-based metric called the shock energy fraction, are used to quantify the strength and prevalence of acoustic shocks within waveforms recorded 10–305 m from a tethered military aircraft. The derivative skewness is more sensitive to the presence of the largest and steepest shocks, whereas the average steepening factor and shock energy fraction tend to emphasize aggregate behavior of the entire waveform. These metrics are applied at various engine conditions, over a wide range of angles and distances, to assess the growth and decay of shock waves. This paper represents the first time that the development of these metrics is shown from the near field to the far field, out to 305 m. The responses of these metrics point to significant shock formation occurring through nonlinear propagation out to 76 m from the microphone array reference position. Although these strongest shocks decay past 35 m, continued shock formation and atmospheric absorption can make the steepened nature of the waveform more prominent out to 305 m.

Nomenclature

C_v	=	coefficient of variation
f	=	frequency, Hz
OASPL	=	overall sound pressure level, dB re 20 μPa
p	=	pressure
r	=	distance from the microphone array reference position, m
t	=	time, s
WPS	=	wavelet power spectrum, Pa^2/Hz
θ	=	angle measured with respect to the aircraft nose
σ_p	=	standard deviation of the pressure waveform
$\sigma_{\partial p/\partial t}$	=	standard deviation of the first time derivative of the pressure waveform

I. Introduction

ONE of the distinctive features visible in waveforms of supersonic jet noise is the presence of acoustic shocks or large sudden increases in pressure. These shocks are often associated with the auditory phenomenon called crackle [1] and serve as an additional source of annoyance within jet noise. Some metrics tied to human perception of noise have been applied to jet noise [2], but some issues arise due to the steepened nature of the shocks [4]. The nature of these shocks and their evolution in the noise field are dependent on their physical properties and origins. Steepened waveforms exist near the source [1,6], but it has also been shown that waveforms from full-scale aircraft continue to steepen and form shocks further away from the source due to nonlinear propagation [7,8]. One of the first indications that nonlinear propagation played a role in far-field effects was a lack of atmospheric absorption in the far field noticed by Pernet and Payne [9] and later by Morfey and Howell [10]. The steepening of waveforms and formation of shocks were also shown by Blackstock [11] to increase at locations farther from the jet noise source though his analysis did not incorporate atmospheric absorption. While the field of nonlinear acoustics has produced many tools for accurately characterizing the nonlinear propagation [12,13], many efforts have vied for metrics to quantify waveform steepening, shock content, and crackle. One of the first attempts was performed by Ffowcs Williams et al. [14] and was based on the statistical measure of skewness of the pressure waveform distribution. Ffowcs Williams et al. defined a distinctly crackling waveform as having a skewness above 0.4. However, because shocks may exist without affecting the skewness of the pressure waveform, defining crackle based on the skewness of the waveform leads to an insufficient definition [6]. A better quantification of waveform steepening and shock content is needed as the ability to quantify the steepened nature of jet noise waveforms enables a correct comparison of these important characteristics between measurement locations, across engine conditions, and among different experimental datasets.

Recent work in quantifying the steepening of a waveform has concentrated on the presence of large derivative values associated with shocks [15,16]. These efforts often rely on metrics calculated from the waveforms. Such metrics may evaluate the time-domain [17] or frequency-domain [10] characteristics of the waveform, and have been applied to full-scale [6] and laboratory-scale [18,19] data. However, one of the issues that arise from the use of metrics is their interpretation. In many cases it is difficult to tell at what point a waveform has steepened sufficiently to qualify as a shock and when it has unsteepened enough to no longer be considered a shock. In addition, some have pointed to the lack of physical meaning of

Presented as Paper 2017-4043 at the 23rd AIAA/CEAS Aeroacoustics Conference, Denver, CO, June 5–9, 2017; received 20 August 2021; revision received 7 January 2022; accepted for publication 11 March 2022; published online 24 May 2022.

*Ph.D. Candidate, Department of Physics and Astronomy, N283 ESC. Student Member AIAA.
†Associate Professor, Department of Physics and Astronomy, N283 ESC. Senior Member AIAA.
‡Part-Time Assistant Professor, Department of Physics and Astronomy, N283 ESC. Member AIAA.
§Postdoctoral Fellow, Department of Physics and Astronomy, N283 ESC. Member AIAA.
¶Research Physicist, Battlespace Acoustics Branch, 2610 Seventh Street, Building 441. Member AIAA.
**Senior Scientist, 29 N Market Street, Suite 700. Member AIAA.
††Senior Principal Engineer, 29 N Market Street, Suite 700. Member AIAA.

metrics [6,20], making it difficult to interpret results and compare between experiments.

Understanding these waveform steepening metrics has been enhanced recently by theoretical and experimental analyses. In model-scale work, Baars et al. [1] have shown values for various metrics in the near-field of model-scale supersonic jet noise in an attempt to locate the source of the shock-like behavior. Others, including Muhlestein et al. [15] and Reichman et al. [16,21], have quantified the connection between shock content and metrics through analytical derivations involving nonlinearly propagating, initially sinusoidal signals and extended the derivations to noise phenomena. This recent work not only helps provide physical context to values seen when comparing metrics, but also points to possible issues when comparing experiments, e.g., relative sampling rates and extraneous noise characteristics.

Investigation into the shock-related metrics continues in this paper with an application to full-scale military aircraft noise measured over a large aperture. Time waveforms, associated spectra, and a wavelet analysis show that steepening in waveforms continues as distance from the source increases. Metrics to be calculated and compared include the skewness of the first time-derivative of the pressure waveform, the average steepening factor (ASF), and a new wavelet-based metric called the shock energy fraction (SEF). This represents for the first time that the SEF wavelet analysis has been applied to military jet noise measurements. In addition, these analyses represent for the first time that a connection has been made between noise measured over such a large propagation distance—from geometric near field to the far field of a military aircraft. These analyses show that shocks and steepened portions of waveforms in the far field of the F-35 are primarily formed through nonlinear propagation.

II. Metrics Indicative of Nonlinear Propagation

Because of the broadband, complex nature of jet noise and its extended source region, it is a challenge to define where nonlinear propagation and shock formation occur. As such, attempts to quantify the strength of shocks within jet noise have often concentrated on nonlinearity metrics, single values expressing the shock content of a waveform. These metrics can help as an easy comparison of the steepened nature of waveforms, but when taken only one at a time may underscore features that are emphasized within other metrics. As such, this paper shows the time-domain metrics of derivative skewness, ASF, and SEF, a new wavelet-based metric, to highlight different aspects of the steepened waveforms.

A. Derivative Skewness

The skewness of the distribution of the first time-derivative of the pressure waveform (estimated here via two-point finite difference) is a statistical measure that assesses the overall steepness of a waveform. The skewness of a distribution is the third standardized moment, defined as

$$\mathrm{Sk}\{x\} = E\left[\left(\frac{x-\mu}{\sigma}\right)^3\right] \tag{1}$$

where μ is the mean of the distribution and σ the standard deviation. Nonzero skewness values, generally, express an asymmetry in a distribution. The large derivative values associated with acoustic shocks result in a derivative distribution in which there are many slightly negative values with relatively fewer, but significantly larger positive values. This type of distribution has a large, positive derivative skewness indicative of steepened waveforms. A positive derivative skewness has been used to show the presence of shocks in both model-scale [1,18] and full-scale [22] analyses.

An advantage of this metric, $\mathrm{Sk}\{\partial p/\partial t\}$, is that it is dependent only on the waveform shape and independent of an arbitrary definition of a shock, though low sampling rates may cause the true derivative skewness to be underestimated [6,16]. Recent analytical work has shown the derivative skewness values for initially sinusoidal signals as the waveform steepens and unsteepens [16]. Using a criterion for classifying shocks based on the rise time of the steepened sinusoid, a wave in the preshock region can be considered shock-like at a derivative skewness of 8.9, whereas a waveform in the postshock region thickens and is no longer classified as shock-like at a derivative skewness of 3.9. Other examples within jet noise confirm that $\mathrm{Sk}\{\partial p/\partial t\}\tilde{5}$ can signify the presence of shocks [6]. As such, this value of $\mathrm{Sk}\{\partial p/\partial t\} \geq 5$ will serve as a threshold to indicate significant waveform steepening and shock content, provided that the sampling frequency exceeds the peak frequency of the waveform by a factor of at least 100.

B. Average Steepening Factor

Another time-domain metric that has been used to quantify waveform steepening is the ASF, defined as the average value of positive derivatives divided by the average value of negative derivatives. This quantity was originally defined as the inverse, the waveform steepening factor $\mathrm{WSF} = 1/\mathrm{ASF}$, but it had the conceptual difficulty of decreasing numerically as steepening increased. Muhlestein et al. [15] derived analytical expressions for ASF for high-amplitude, initially sinusoidal signals, and additionally showed values for nonlinearly propagating noise in a plane-wave environment. A nonsteepened waveform would have $\mathrm{ASF} = 1$, whereas steepened waveforms have higher values. Because the ASF is a linear mean of derivative values it represents trends within the entire waveform more than the derivative skewness, which accentuates the large positive outliers. However, the ASF is also more susceptible to the presence of extraneous noise than the derivative skewness [16]. Like the derivative skewness, ASF has been used in both model-scale [1] and full-scale [23] jet noise applications. It has been shown that in both cases an ASF value between 1.5 and 2 is indicative of the presence of shocks, with an ASF value approaching two suggesting significant shock content [1,23].

C. Shock Energy Fraction

Though time-domain metrics can show the steepening that comes about as a result of nonlinear propagation, the auditory perception of shocks, crackle, is tied to increased high-frequency content. The steepening of shocks in the time domain results in spectral broadening in the frequency domain, as energy is transferred from the peak frequency region to higher frequencies. As such, this metric is being introduced to compare the frequency content of shocks with the rest of the waveform. Although frequency content is often shown using the more familiar Fourier transform, a wavelet transform has been used in lab-scale jet noise analysis as a frequency-domain technique that also gives temporal resolution [1]. The wavelet analysis involves a convolution of the waveform with a wavelet shape to give spectral information that is time-resolved as well. The absolute value of this convolution, similar to a Fourier transform, may be squared to give the wavelet power spectrum (WPS), which if averaged over time approximates the autospectrum. Many types of wavelets exist, but for this paper the Morlet wavelet is used to mirror previous studies [1], where the wavelet analysis was used to show the association of high-frequency noise with shock waves and to investigate the near field of model-scale jet noise for evidence of shock wave origins. An example of the wavelet transform applied to a waveform is shown in Fig. 1. The example waveform, of F-35A noise for 150% engine thrust request (ETR) at $r = 76$ m and $\theta = 135°$, is shown in Fig. 1a and has multiple shocks visible. The corresponding wavelet transform is shown in Fig. 1b. In the WPS an increase in high-frequency energy is visible at times corresponding to rapid increases in pressure. This high-frequency energy in the WPS is indicative of acoustic shocks.

To also incorporate the high-frequency energy associated with shocks, Baars and Tinney [1] proposed a metric involving the wavelet transform. This metric, a percent energy gain, used a shock detection algorithm to find sharp compressive regions of the waveform. This algorithm defined a shock as a derivative value above $\sigma_p/\Delta t$, where σ_p is the standard deviation of the pressure waveform and Δt is the time between samples. After a shock was identified, which corresponded to a single point, the temporal duration of the entire shock was defined as the time from the local waveform minimum directly

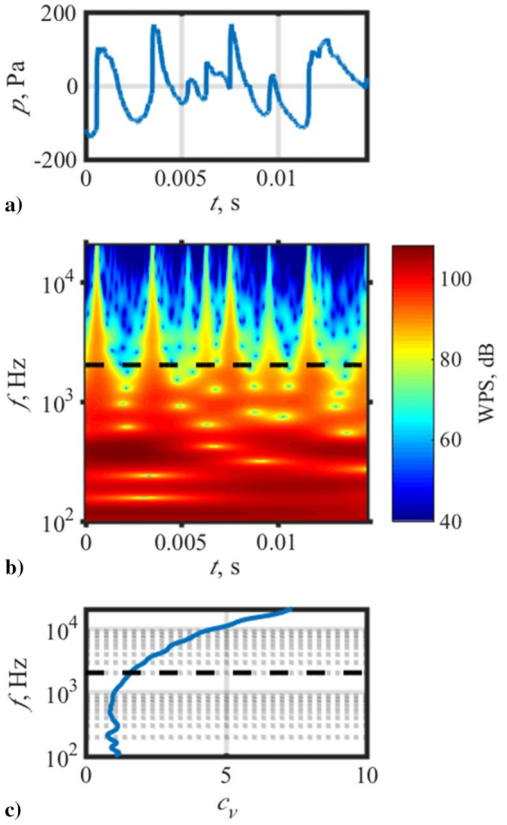

Fig. 1 An example a) shock-containing waveform, b) wavelet transform of the waveform, and c) coefficient of variation for each frequency.

before the shock to the local waveform maximum directly after the shock. The algorithm then compiled an average spectrum of the WPS at the identified shocks. The average A-weighted spectrum of the shocks was compared with the A-weighted spectrum of the entire waveform to determine the percent increase in energy due to the presence of shocks. This method has many interesting components, but some changes can help results agree more fully with expected shock behavior. One potential flaw in the percent energy gain was the application of the A-weighting to both the WPS and the waveform spectrum to correlate more closely with human perception. However, the A-weighting can reduce the effect of higher-frequency noise. The shock detection algorithm was also shown in their paper [1] to be invalid for some propagation angles, which likely caused anomalous results. In addition, the spectral comparisons were performed based purely on the WPS, disregarding the number of shocks present in a waveform. This means that one shock within a 10 s waveform may be given the same emphasis as a waveform with 100 shocks per second.

To improve upon the foundation provided by Baars and Tinney, a new metric is proposed, the SEF. This metric bears similarities to the percent energy gain but with key differences. First, this new shock detection threshold (which is defined more specifically in the Appendix) is based on $\sigma_{\partial p/\partial t}$, the standard deviation of the waveform derivative values. This emphasizes large derivative outliers, common for acoustic shocks, while minimizing the effects of high-frequency noise that potentially contaminated the shock detection algorithm used previously. A threshold is set and portions of the waveform with derivative values above this threshold are considered to be shocks. Rather than compare spectra directly, a new approach is used that accounts for time in a manner similar to sound exposure level (SEL) [24]; both the WPS and the duration of time associated with the number and length of shocks are used to define the SEF.

The primary difference in the WPS between the shock-containing portions and the remaining sections is the prominent presence of high-frequency sound, as seen in Fig. 1b. The A-weighting applied in Ref. [1] minimized the effects of low-frequency noise, which remains consistent throughout the waveform and would otherwise dominate the higher-frequency differences that occur at a much lower decibel level. In contrast, the SEF is defined as an integral, not over the entire frequency range, but starting at a low-frequency limit. The justification for this lower-frequency limit can be seen in the coefficient of variation, C_v, shown in Fig. 1c as a function of frequency f. This coefficient is the normalized standard deviation of a function $C_v = \sigma/\mu$, where σ is the standard deviation and μ is the mean value. Though ill-defined for many acoustics applications due to the abundance of zero-mean processes, C_v can be useful for energy-based applications (where explicitly non-negative values can be assumed) to show variation in a quantity. For the example waveform, C_v is shown to vary little below 1 kHz, and increases more rapidly above 2 kHz; C_v increases due to the large difference in WPS values between sections of the waveform with and without shocks. Using this as motivation, the WPS is integrated only above 2 kHz, roughly 10 times the peak frequency, to show the fraction of high-frequency energy associated with shock waves present in the waveforms.

With the above considerations, the SEF is defined as

$$\mathrm{SEF} = \frac{\sum_{t_{\mathrm{shocks}}} \sum_{f_{\min}=2\,\mathrm{kHz}}^{f_{\max}} \mathrm{WPS}\Delta f \Delta t}{\sum_{t} \sum_{f_{\min}=2\,\mathrm{kHz}}^{f_{\max}} \mathrm{WPS}\Delta f \Delta t} \tag{2}$$

SEF is bounded between 0 and 1: SEF = 0 means that no high-frequency energy is found in the shocks, or that no shocks are observed above the detection threshold, and SEF = 1 m eans that no high-frequency energy is observed outside of shock-containing regions of the waveforms. The behavior of SEF is compared to the derivative skewness and the ASF by application to the F-35 jet noise measurements.

III. Measurement Details

A. Setup

The dataset examined in this paper was collected at Edwards Air Force Base, September 5, 2013. The experiment has been extensively described by James et al. [24], but pertinent details are given here. Noise measurements were taken as a tethered F-35A was cycled through power settings ranging from idle to 150% engine thrust request (ETR), or maximum afterburner. Each engine condition was measured multiple times throughout the course of measurements. The 235 unique measurement locations, chosen in accordance with ANSI S12.75, represent the largest full-scale dataset to date, with microphones located as close as 10 m from the shear layer out to 1220 m away from the microphone array reference position (MARP), located 6.6 m behind the nozzle at (0, 0) in Fig. 2. Microphones were arranged in either line arrays parallel to the jet centerline, or in semicircular arcs centered at the MARP. As most of the noise generated by supersonic jets is emitted from the turbulent mixing that occurs behind the jet, the MARP represents a rough estimate of source location for many frequencies of interest. For arcs at 38 m and beyond, arc spacing of 5° between microphones was used in the direction of peak radiation, between 120 and 160°. The ground surface close to the MARP was the concrete and asphalt aircraft pad, whereas terrain beyond roughly 50 m transitioned to a dry lake bed and desert ground, providing a rigid ground surface.

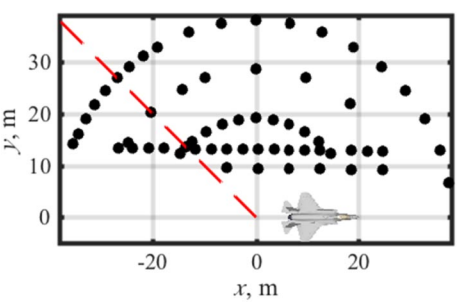

Fig. 2 Microphone measurement positions within 38 m of the MARP. The dashed red line shows the $\theta = 135°$ radial.

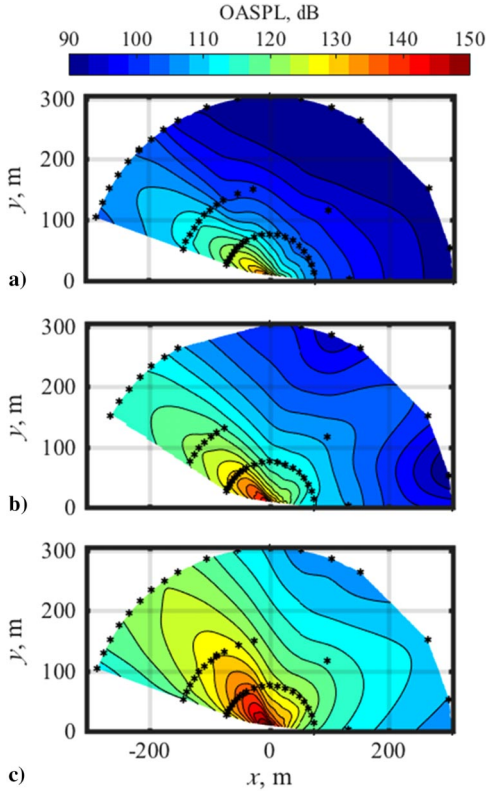

Fig. 3 OASPL within 305 m of an F-35A at a) 50% ETR, b) 75% ETR, and c) 150% ETR.

The microphone locations within 38 m of the aircraft are shown in Fig. 2, with the aircraft also included and shown to scale. Microphone locations beyond 38 m are shown in later plots. In the areas of maximum acoustic pressure, 6.35 mm (1/4″) microphones were used, with sampling rates of either 192 or 204.8 kHz. At 305 m, in the forward direction, waveforms were captured at measurement locations from 0 to 40° and 60 to 80° using sound level meters. The meters recorded time-history Waveform Audio File Format (wav) files at a sampling rate of 51.2 kHz. Measurements were conducted between 3:00 and 9:00 a.m. local time, with temperature varying between 19.4 and 23.1°C, relative humidity between 37.6 and 45.7%, and an average wind speed of 3.3 kts.

B. Overall Sound Pressure Level

The directivity of jet noise and its dependency upon engine conditions are key features of jet aircraft noise as shown in Fig. 3 for 50, 75, and 150%. Microphone locations within 38 m of the MARP are shown in Fig. 2, and microphone locations at 76, 152, and 305 m are shown as black dots on the plot of the overall sounds pressure level (OASPL) in Fig. 3, with a polar interpolation scheme being used to fill in the areas between microphone locations. More engine conditions may be seen in Ref. [30] for the F-35B, which is acoustically similar to the F-35A shown here. In addition to the increase in OASPL seen at higher engine conditions, a shift in directivity is also observed. The OASPL peaks at 145° at 50% ETR, whereas the directivity shifts forward, toward the nose of the aircraft, with increasing engine power. At 75% the OASPL peaks at 135° from the aircraft nose with the origin at the MARP, whereas at 150% it peaks at 125°. In all cases, the far-field decay in OASPL is in line with expectations due to geometric spreading, though this will be explored further in Sec. V.

IV. Evidence of Shock Formation

The shock quantification metrics introduced in Sec. II are shown over the entire measurement aperture in this section. As the data were recorded at each engine condition multiple times, the average value between datasets is shown here, averaged over five measurements at each engine condition. The results are shown at 50, 75, and 150% ETR. As the nozzle diameter is on the order of 1 m, the spatial maps extend to roughly 300 nozzle diameters, farther than most laboratory-scale measurements [1,25], though some far-field laboratory-scale measurements do exist [26].

A. Waveform Characteristics

As an introduction to shock formation due to nonlinear propagation, normalized waveforms are considered (Fig. 4), at distances of 19, 29, 38, 76, and 152 m along the 135° radial, shown as a red line in Fig. 2. These waveforms are shown as a function of retarded time to demonstrate the evolution of waveform features with distance. Because the waveforms are plotted on a normalized scale to accentuate waveform evolution with distance, the maximum pressure and derivative values are shown in Table 1.

Significant differences exist between the waveforms measured at 19 and 29 m, including small shocks present at 19 m (in particular between 0.005 and 0.01 s) and other waveform shape issues that are likely due to near-field propagation effects. However, the significant features in the waveform are largely preserved from 29 out to 305 m, and differences can mainly be seen due to nonlinear steepening. The consistency between 29 and 305 m indicates that this measurement radial is also a propagation radial. The most noticeable change occurs near 0.015 s, as the steepened portion of the waveform forms a distinct shock by 38 m from the MARP. This shock persists all the way out to 305 m, though it does decay slightly with respect to the rest of the waveform.

Though the largest shock just after 0.015 s is well-defined by 38 m from the MARP, nonlinear propagation continues to affect the waveform out to 152 m. In particular, smaller amplitude sections of the waveform, which are clearly not shock-like at 76 m, are significantly steeper at 152 m (around 0.01 s, for example), though they begin to slightly thicken by 305 m. Similar behavior was observed in the propagation of noise from another aircraft by Gee et al. [27] for a lower-power engine condition—the largest features steepen and form shocks by 38 m, but smaller-amplitude sections of the waveform continue to steepen beyond this distance. These waveforms show that shock formation within noise does not occur at a specific distance from the source but is a continuous process that is dependent on the amplitude and frequency content within each section of the waveform. To accurately characterize the nonlinear propagation and shock formation of entire waveforms, it is useful to express the steepness and shock characteristics of an entire waveform in single-value metrics.

While the evolution of the waveform and its time derivative provide evidence of nonlinear propagation producing shocks in the far field of jet noise, it is difficult to know if the 0.02 s portion represents the entire waveform. One way to examine the shock content of the entire (30 s) waveform is a two-dimensional histogram of derivative values, introduced by McInerny and Ölçmen for rocket launch data [28]. In the plots shown in Fig. 5, each subplot represents one waveform from Fig. 4. Each waveform is then broken up into sections (as little as two consecutive points) where the pressure is continuously increasing. The maximum derivative within each section is plotted on the y axis against the total pressure increase over the section, Δp, on the x axis. In a slight change from McInerny and

Table 1 Maximum pressure and derivative values for plots in Fig. 4

Distance, m	Maximum pressure, Pa	Maximum derivative, MPa/s
19	1,805	64
29	1,444	92
38	1,364	105
76	630	57
152	263	12
305	85	4.1

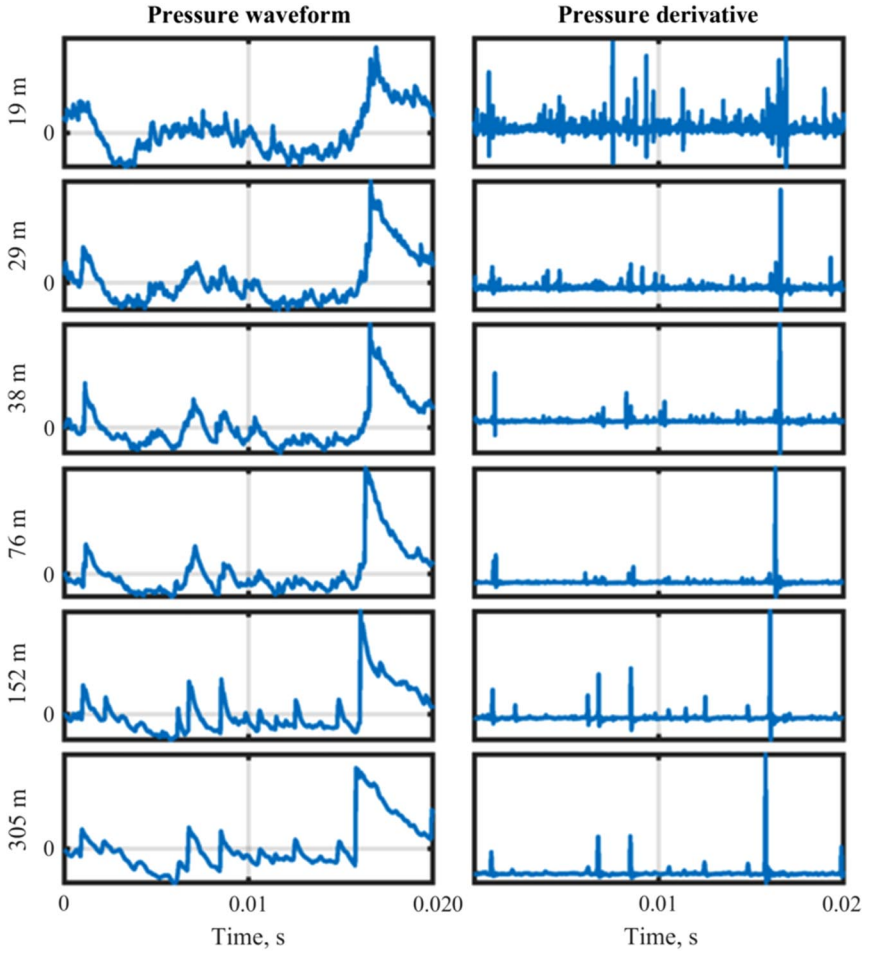

Fig. 4 Normalized, time-aligned waveforms and their normalized derivatives at 150% ETR along the 135° radial (red line in Fig. 2) at various distances from the MARP.

Ölçmen's original plots, the results here are shown in a bivariate histogram plot, similar to Muhlestein [29], to show not only where derivative values are occurring, but also how many of them occur. The plots are also normalized according to σ_p and $\sigma_{\partial p/\partial t}$ to allow for an easy comparison between relative importance of shocks.

A few guiding lines are present in each of the subplots in Fig. 5 to help with understanding. The dashed black line represents a two-point shock, where the entire rise Δp occurs between two samples. Though theoretically this should be the limiting case, bin discretization causes some data points to appear above this line. For large Δp, it is safe to say that a two-point shock means that the sampling rate is inadequate to accurately characterize shock characteristics. The red dashed line, which corresponds to the line plotted by McInerny and Ölçmen, is a factor of two lower than the black line and represents a three-point shock. This line is more indicative of limiting behavior for large shocks due to sampling rate and low-pass filters implemented by a data acquisition system. Finally, the cyan and green lines represent the expected rise times when shock behavior is dominated by different regimes of absorption. For the longer rise times associated with the green line, absorption is characterized by a combination of thermoviscous losses and relaxation of both nitrogen and oxygen. For shorter rise times (the cyan line) the relaxation of nitrogen can be neglected. A more detailed explanation of the phenomena can be found in McInerny and Ölçmen's paper.

As the plots in Fig. 5 show increases in pressure from the entire waveform, shocks can be compared with other, more gradual increases to illustrate shock evolution relative to the rest of the waveform. In Fig. 5a, 19 m from the MARP, there are a small number of two-point shocks with a large amplitude Δp. These two-point shocks gradually disappear between Figs. 5a and 5d, but even out to 76 m in Fig. 5d the largest amplitude Δp are still three-point shocks, indicating that sampling rate and measurement effects are likely limiting the rise time of these largest shocks. At 76 m significantly more shocks have formed than were present at closer distances, as evidenced by the change in color. At 152 and 305 m the shocks are below the red dashed line, indicating that sampling rate is likely sufficient for these distances. Another important behavior is the relative increase of stronger shocks. As near-field shocks disappear and coalesce at closer distances in Fig. 4, the remaining larger features in the far field result in a larger number of points with $\Delta P > \sigma_p$ with increasing distance. This is especially apparent in Figs. 5e and 5f, where there are a large number of larger-amplitude shocks. This behavior illustrates the steepening of smaller shock features seen in Fig. 4 at distances of 152 and 305 m. These features show many of the behaviors identified in the discussion of Fig. 4, but in the context of the entire waveform, and prepare us for an informed discussion of the metrics introduced earlier.

B. Derivative Skewness

The presence and strength of the largest acoustics shocks are readily shown by the derivative skewness, as evident in Fig. 6 at 50, 75, and 150% ETR. While the angular resolution of the data is every 5° in the peak radiation direction, the radial distribution in the far field is still rather coarse, with points at 76, 152, and 305 m. Though the polar interpolation scheme used is more likely to represent the physical phenomena present than a Cartesian scheme, there are still likely interpolation effects that accentuate the dip seen between 152 and 305 m, and more measurements are needed to precisely characterize the behavior. However, the measured behavior does indicate that at 150%, the derivative skewness decreases between 76 and 152 m, then slightly increases between 152 and 305 m.

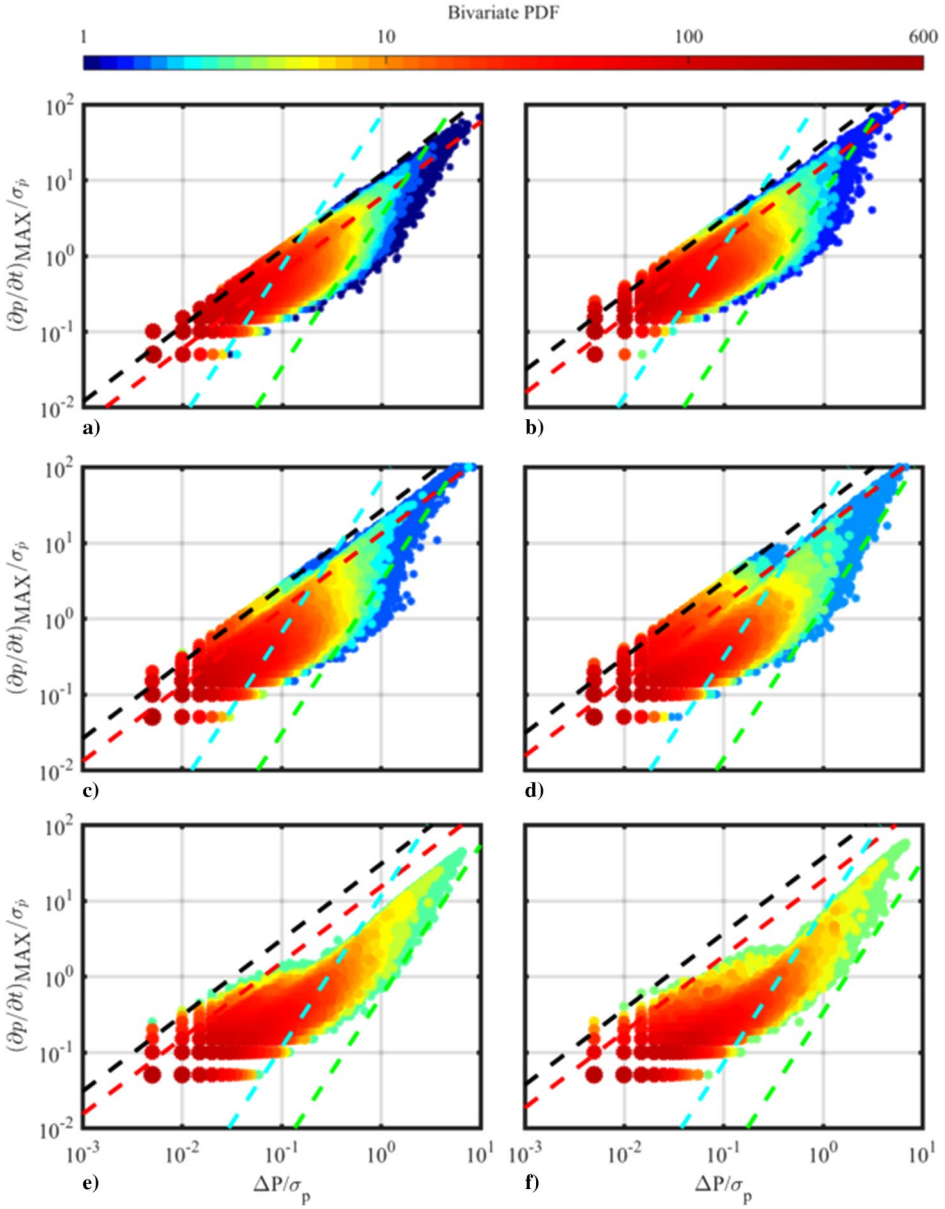

Fig. 5 Bivariate histogram plots of pressure increases vs the maximum derivatives at a) 19 m, b) 28 m, c) 38 m, d) 76 m, e) 152 m, and f) 305 m at 150% ETR. Dashed lines indicate two-point shocks (black), three-point shocks (red), and expected rise times when shock behavior is dominated by different regimes of absorption (cyan and green).

The derivative skewness values shown in the near field in Fig. 6 are similar to those seen in other measurements of F-35 variants. Similar values were shown for the F-35B in Ref. [30]. Some differences are seen when comparing the values at 50 and 150% with those reported by Gee et al. [6] for the F-35 AA-1. These differences are largely explained by the differences in sampling frequencies between the current study (192 or 204.8 kHz) and for the F-35 AA-1 study (96 kHz). When the waveforms from the current study are resampled, the disagreements in large part disappear. For example, at 10 m from the MARP at 130°, the resampled derivative skewness is 5.5, in agreement with findings of Gee et al. At 38 m the resampled derivative skewness value drops from 22 to 16, which is closer but still slightly elevated from the F-35 AA-1 result of 12.

Derivative skewness values depend on the engine power conditions. The derivative skewness values at 50%, shown in Fig. 6a, are not indicative of the presence of shocks. The 50% ETR power condition derivative skewness peaks at a value of $\mathrm{Sk}\{\partial p/\partial t\} = 2.5$, below the threshold of ∼5 that indicates significant shock content [16]. The near-field behavior of derivative skewness at 75 and 150% ETR differs greatly from that at 50%. Although not clear in the figure, at the closest measurement locations to the MARP along the direction of peak OASPL, the derivative skewness is approximately 7 or 8 for both 75 and 150% ETR. In both cases, the derivative skewness exceeds 20 at 76 m, and then decreases. This finding is in agreement with the behavior seen in Fig. 4 that the largest shocks are forming by 76 m from the MARP. However, important differences remain between 75 and 150% ETR. The derivative skewness reaches a slightly higher value at 150% of 27, compared with 25 at 75%, though this difference is not likely significant. In addition, higher derivative skewness values persist over longer distances at 150%. At 305 m, the derivative skewness at 75% has dropped below a value of 10, whereas it remains above 15 at 150%. Both of these values, while lower than the peak derivative skewness seen at 76 m, still indicate the presence of significant shocks in the jet's far field.

C. Average Steepening Factor

While the derivative skewness accentuates the positive outliers and indicates the presence of the strongest shocks, the ASF is instead a measure of average behavior and thus less sensitive to the less frequent but extremely large derivative values. Similar to the previous plots, at 50% ETR the low ASF values shown in Fig. 7a indicate that although the jet noise is steepening slightly, it does not contain

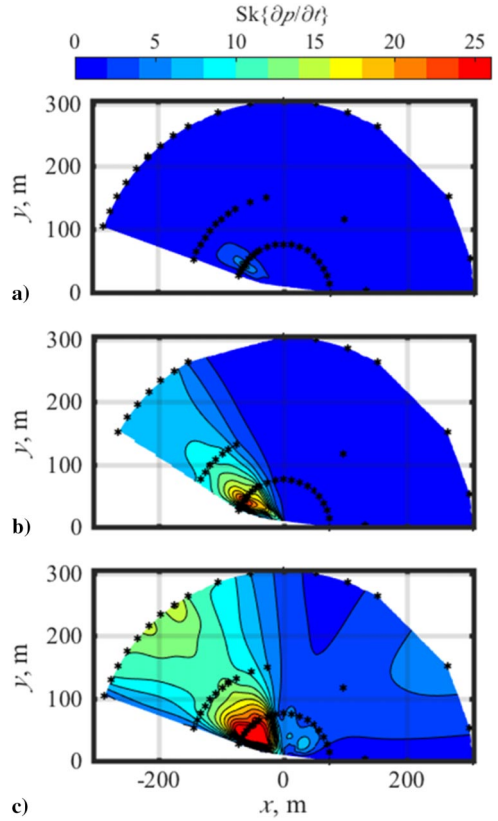

Fig. 6 Derivative skewness near an F-35A at a) 50% ETR, b) 75% ETR, and c) 150% ETR.

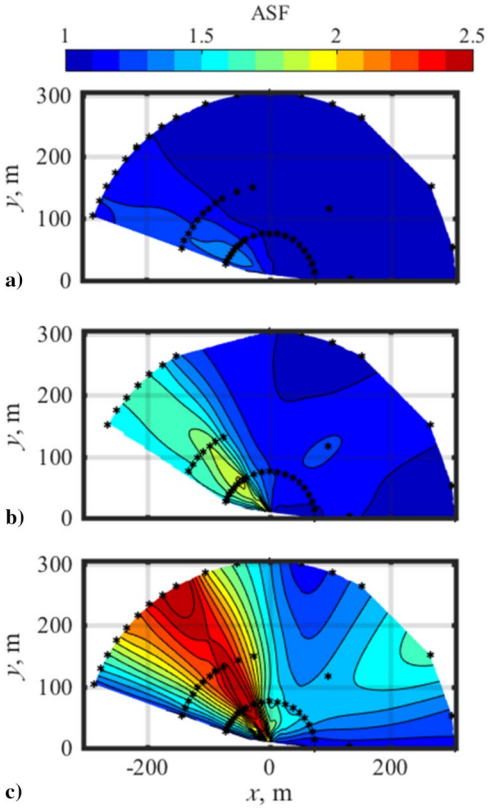

Fig. 7 ASF within 305 m an F-35A at a) 50% ETR, b) 75% ETR, and c) 150% ETR.

shocks. However, at 75% the ASF (in Fig. 7b) reaches values above 2 in the direction of peak OASPL, indicative of more significantly steepened waves. The ASF is significantly higher at 150% ETR (in Fig. 7c), reaching values of 2.5. Since ASF $= 1$ indicates a symmetric distribution of derivative values, the comparison of ASF values should be relative to 1. Thus, a value of 2.5 is roughly 50% more than a value of 2, or $(2.5 - 1) = 1.5 \times (2.0 - 1)$. The peak ASF values are seen near the peak OASPL values, occurring at 140, 130, and 120° at 50, 75, and 150% ETR, respectively, echoing the forward shift seen in previously observed behavior [23].

One important clarification is that the behavior of the ASF is highly dependent on the type of noise being considered. In the analytical paper describing ASF by Muhlestein et al. [15], a value of two was reached by initially Gaussian noise without significant shocks present. However, the waveforms shown here, despite having comparable ASF, are shown to have significant shocks by visual inspection and the high derivative skewness values.

Significant changes in spatial variation in ASF are seen between the three engine conditions. At 50%, a slight increase is seen through propagation away from the jet. At 75% the increase is much more dramatic, peaking at 76 m before decreasing out to 305 m. However, at 150% the ASF continues to increase along propagation radials even out to 305 m. Because the ASF represents a linear average of positive derivatives to the linear average of negative derivatives, it does not accentuate the largest shocks, which cause the derivative skewness to peak at 76 m. The continually increasing ASF out to 305 m at 150% ETR is due to continued nonlinear propagation, as seen by comparing the waveforms in Fig. 4. The nonlinear effects are evident in continued shock formation, general waveform steepening, and the persistence of shocks coupled with dissipation of high-frequency energy not associated with shocks due to atmospheric absorption. Over a distance of 100 m at the measurement conditions listed above, the expected atmospheric absorption at 5 kHz is roughly 4.7 dB/100 m, 11.5 dB/100 m at 8 kHz, and increasing roughly proportionally to the frequency squared at higher frequencies. This means that at distances over 100 m from the source, frequency content at frequencies above 10 kHz is in great measure due to the shocks present in the waveform. As designed, the ASF indicates the average strength of the shocks relative to the overall signal; ASF continues to increase with distance as nonlinear propagation effects continue to steepen the high-amplitude portions of the waveform and atmospheric absorption reduces the lower-amplitude, high-frequency portions of the waveform.

D. Shock Energy Fraction

If the attenuation of high-frequency energy not associated with shocks is a cause of steadily increasing ASF values, this should be readily seen in the SEF, since the SEF shows the fraction of high-frequency energy (above 2 kHz) associated with shocks. Spatial maps of the SEF are displayed in Fig. 8 at 50, 75, and 150% ETR. In Fig. 8a, the low SEF at 50% ETR again confirms the lack of significant shocks in the waveforms, though the values are nonzero in the direction of peak OASPL. Similar to the other metrics, a large change in metric behavior is seen when comparing 50 and 75% ETR. At 75% (Fig. 8b), the increasing prominence of shocks is evident as the SEF increases with distance to values above 0.1, meaning that the infrequent shocks contribute more than 10% of the energy above 2 kHz. At 75% ETR the SEF begins to decrease from 152 to 305 m, but in contrast the 150% ETR in Fig. 8c continues to increase to 305 m, where it reaches values of above 0.12. These values suggest that at 150% ETR the acoustic shocks are a main contributor of high-frequency energy at these distances from the source; high-frequency energy not associated with the shocks has likely been significantly attenuated due to atmospheric absorption. This attenuation is also seen when comparing the closest waveforms in Fig. 4 with those measured at farther distances. In addition, the growth in SEF with distance points to the persistence of nonlinear propagation and continued transfer of energy to higher harmonics. If nonlinear propagation were negligible, the SEF would remain constant or decrease as high-frequency energy is absorbed at all sections of the waveform equally, similar to 50% ETR.

At 75% ETR, the decrease of SEF between 152 and 305 m indicates that shocks are decaying and reducing in prominence. The increase in SEF at 150% points to continued nonlinear propagation and increased shock prominence when compared with the rest of the waveform out to 305 m from the MARP.

E. Spatial Trend Summary

Though the above analyses show the prominence of shocks within jet noise in different ways, together they form a cohesive picture of continual nonlinear propagation away from the source of jet noise. At 150% ETR, all of the metrics suggest that the strongest shocks are not present immediately at the source but form through nonlinear propagation. The derivative skewness, emphasizing the largest positive outliers, peaks near 76 m, at which point the largest shocks have formed and begin decaying. However, because a noise signal is a complicated amalgamation of various frequencies rather than a simple sinusoid, shock formation is not limited to a particular spatial range. Though the largest shocks form by 152 m, overall waveform steepening and smaller shock formation continue to drive an increase in values of ASF at 150% ETR. In addition, the rise in ASF is attributable to the decay in lower-amplitude, high-frequency energy not associated with shocks due to atmospheric absorption. This increase in the relative prominence of the shocks is also seen in the growth of SEF with distance. The evolution of these nonlinearity metrics over this large spatial aperture provides conclusive evidence that although some shocks exist in the near field of the jet noise source, the strongest acoustic shocks form by 76 m and nonlinear propagation persists out to at least 305 m from the MARP.

V. Nonlinear Metrics Along Radials

Though the spatial maps presented in Sec. IV are an efficient way to highlight trends associated with directivity and distance, there are advantages in considering propagation along individual measurement radials. Radial comparisons provide an easier way to see trends across engine conditions and show metric values at specific points without interpolation effects. Such comparisons allow for inspection of specific features, such as the dip in derivative skewness seen in Fig. 6, as well as a more quantitative comparison of values between engine conditions. Presented in this section are plots of the metrics considered in Sec. IV as a function of distance along a single radial. These metric value, shown in Fig. 9, are not from a single measurement, but an average of measurements throughout the experiment. The metric values are compared across engine condition to establish and reinforce trends seen in the spatial maps, including the growth of the shocks near the jet source and continued shock formation and propagation into the far field.

This section presents plots of the various metrics as a function of r for the same three engine conditions shown above. At each engine condition, the selected radial displayed corresponds to the angle in the 305 m arc at which the greatest OASPL is measured: 145, 135, and 125° at 50, 75, and 150% ETR, respectively. The different radials account for the differences in the location of data points in the plots of derivative skewness, ASF and SEF shown in Fig. 8, as well as the OASPL in Fig. 8a. Results shown are an average over the 2-day course of measurements.

The derivative skewness displayed in Fig. 8 shows a marked peak at 76 m across all engine conditions. Although the derivative skewness values at 50% do not suggest the presence of significant shocks, the 75% derivative skewness peaks at 76 m with a value of 20. After this point the derivative skewness decreases to 12 at 152 m and further decreases to 10 at 305 m. In contrast, the 150% derivative skewness peaks at 76 m with a value of 28, decreases to a value of 15 at 152 m, and then rises again to 18 at 305 m. The large decrease between 76 and 152 m is likely due to a combination of effects, including propagation through a refracting, turbulent atmosphere, and the presence of vegetation in the propagation path. However, these changes affect the derivative skewness more than the ASF, which is shown to rise continually with distance at 150% ETR in Fig. 8c. The continual rise of ASF and slight increase in derivative skewness between 152 and 305 m point to increased prominence of shocks in the waveform

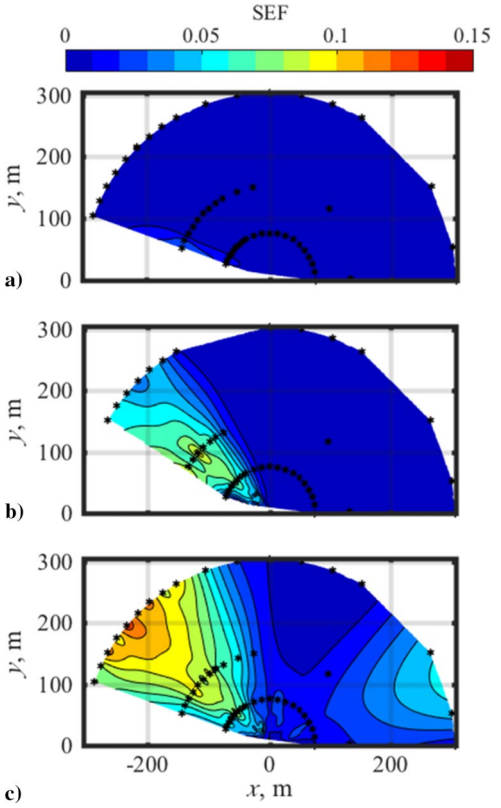

Fig. 8 SEF near an F-35A at a) 50% ETR, b) 75% ETR, and c) 150% ETR.

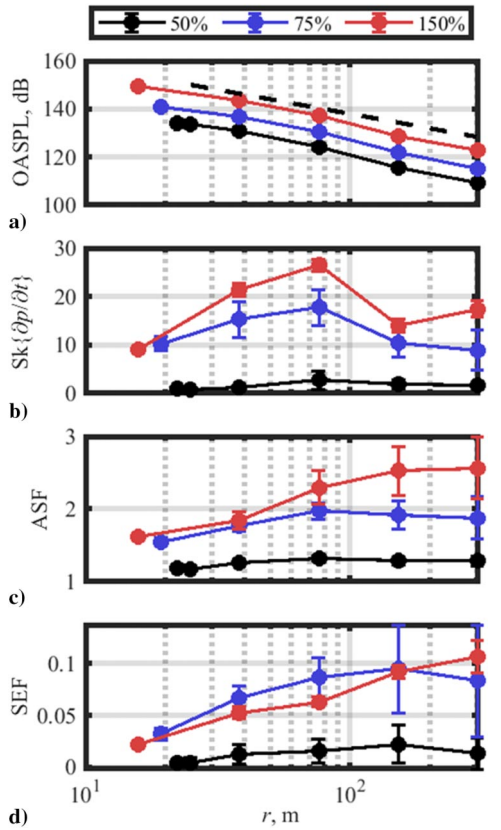

Fig. 9 The a) OASPL, b) derivative skewness, c) ASF, and d) SEF along the peak radiation angle at 50%, 75%, and 150% ETR, with error bars showing standard deviation.

at far distances. The continued increase of ASF out to 305 m is in part due to absorption of high-frequency noise not associated with acoustic shocks. At closer distances, this "background" high-frequency noise creates large positive and negative derivatives that lower both the derivative skewness and ASF below what examination of the shock content in the waveform suggests. However, as this lower-amplitude high-frequency energy propagates and is attenuated through atmospheric absorption, the remaining shocks are accentuated in the ASF and SEF.

The attenuation of high-frequency energy is also apparent in plots of the SEF, shown in Fig. 8d. The SEF at 50% remains more or less constant, whereas at 75 and 150% the SEF grows with distance to 152 m. At 75%, SEF decreases slightly from 152 to 305 m; this decrease appears to be related to a decrease in the number of shocks. However, at 150% the SEF is, similar to the ASF in Fig. 8c, increasing with distance out to 305 m, confirming the reduction in high-frequency energy not associated with shocks. One point to mention is that the SEF is higher at most distances for 75% than 150%, indicating that the shocks are more significant in terms of high-frequency contribution. This is likely due to a combination of effects, including different directivity at the two engine conditions, the number of shocks, and different spectral content. Though the derivative skewness and ASF indicate that shocks are stronger at 150% than at 75%, the SEF informs us that the shocks at 75% contribute more to the high-frequency content of the entire waveform at 152 m and closer.

VI. Conclusions

The various nonlinearity metrics considered in this paper point to the conclusion that nonlinear propagation is an important factor in the near-, mid-, and far-field environments of military jet noise. Though some significant shocks exist at the closest measurement locations at roughly 10 m from the MARP, the waveforms steepen and form shocks through nonlinear propagation. The derivative skewness indicates that the strongest shocks form by 76 m, then slightly thicken at greater distances. The continued growth of ASF points to nonlinear propagation out to at least 305 m, likely due to the persistent steepening of smaller features in the noise. The wavelet-base metric SEF appears to be a useful nonlinearity metric showing the relative importance of shocks in high-frequency energy. For the F-35, the increase in SEF with distance indicates that high-frequency energy not associated with shocks is attenuated through linear atmospheric absorption. These analyses show that continued shock formation and atmospheric absorption can make the steepened nature of the waveform more prominent out to 305 m.

Appendix: Shock Definition Thresholds

One question raised by the visual inspection of waveforms is how to define and identify shocks. In periodic signals, a shock wave is often defined based on the rise time of the shock relative to the period of the signal. However, in noise signals this definition is not valid, and instead a shock will be defined based on how large a derivative is relative to the distribution of all derivative values. Because the most important feature of a shock is the rapid rise, a threshold based on the standard deviation of the derivative $\sigma_{\partial p/\partial t}$ can be used as a minimum value, above which the derivative is considered a shock. To better illustrate which features are included in different shock definitions, the normalized waveforms shown in Fig. 4 are shown again in Fig. A1 with specific shocks highlighted. The shocks are color-coded according to the minimum threshold that they satisfy; i.e., a shock that satisfies the threshold $15\sigma_{\partial p/\partial t}$ also satisfies all thresholds below it. It can be seen that at the closest measurement locations more shocks are present, but that the majority of shocks are smaller, satisfying the threshold of $3\sigma_{\partial p/\partial t}$ or $5\sigma_{\partial p/\partial t}$, whereas at further distances such as 152 and 305 m there are fewer shocks, but they are now the most notable features of the waveform. This may suggest that although nonlinear propagation is the dominant factor behind waveform steepening in the far field, the mechanisms responsible for the shocks in the near field may be

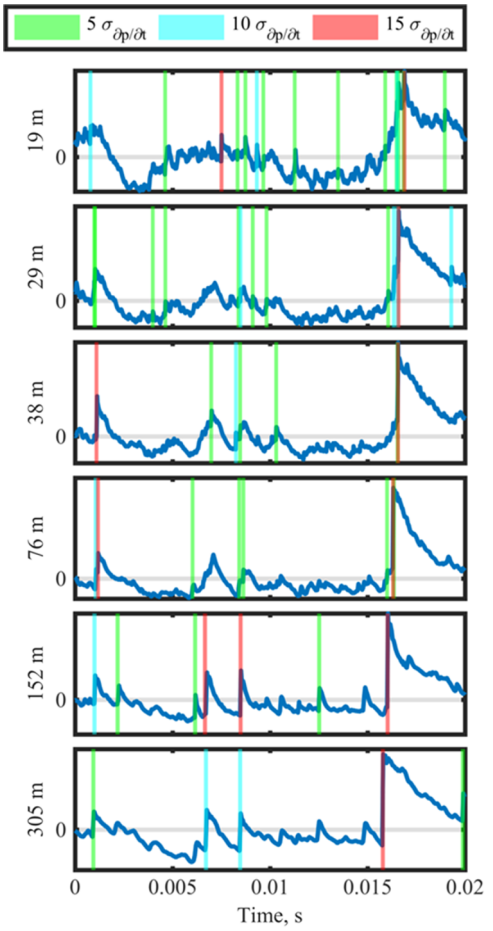

Fig. A1 Shocks in the 150% ETR waveforms from Fig. 4, categorized by strength.

different. The shocks highlighted in Fig. A1 also suggest that while a threshold of $15\sigma_{\partial p/\partial t}$ does capture the most significant shocks, it may omit some significant features, and thus a threshold of $10\sigma_{\partial p/\partial t}$ is preferable.

The SEF is dependent on shock threshold, and so it is logical to investigate how the behavior of the SEF changes with the definition of shock thresholds. As more or fewer sections of the waveform are identified as shocks, how does the WPS associated with shocks change? This question is answered in Fig. A2, where the SEF at 150% along 135° is plotted for various thresholds, ranging from $3\sigma_{\partial p/\partial t}$ to $15\sigma_{\partial p/\partial t}$. Though the SEF for higher thresholds is predictably lower as fewer points are included, the same general trends apply in all cases. The SEF continues to increase out to 305 m in all cases, with the exception of $15\sigma_{\partial p/\partial t}$, which peaks at 76 m.

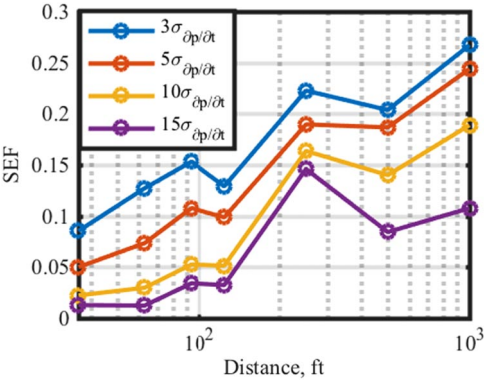

Fig. A2 The SEF at an ETR of 150% and 135° as a function of distance for various shock thresholds.

This serves as evidence that even though the amplitude of the SEF may vary with threshold, the trends remain that out to 305 m shocks become relatively more important in terms of high-frequency content.

Acknowledgments

The authors gratefully acknowledge funding for the measurements, provided through the F-35 Joint Program Office and Air Force Research Laboratory. (Distribution A: Approved for public release; distribution unlimited; Cleared 07/21/2020, JSF20-612.) B. O. Reichman was funded through by an appointment to the Student Research Participation Program at the U.S. Air Force Research Laboratory, 711th Human Performance Wing, Human Effectiveness Directorate, Warfighter Interface Division, Battlespace Acoustics Branch administered by the Oak Ridge Institute for Science and Education through an interagency agreement between the U.S. Department of Energy and USAFRL.

References

[1] Baars, W. J., and Tinney, C. E., "Shock-Structures in the Acoustic Field of a Mach 3 Jet with Crackle," *Journal of Sound and Vibration*, Vol. 333, No. 12, 2014, pp. 2539–2553 https://doi.org/10.1016/j.jsv.2014.01.008

[2] Krothapalli, A., Venkatakrishnan, L., and Lourenco, L., "Crackle—A Dominant Component of Supersonic Jet Mixing Noise," AIAA Paper 2000-2024, 2000.

[3] Brouwer, H. H., "On the Effect of Nonlinear Propagation on Perceived Jet Noise Levels," *Aerospace Science and Technology*, Vol. 12, No. 1, 2008, pp. 74–79. https://doi.org/10.1016/j.ast.2007.10.010

[4] Gee, K. L., Swift, S. H., Sparrow, V. W., Plotkin, K. J., and Downing, J. M., "On the Potential Limitations of Conventional Sound Metrics in Quantifying Perception of Nonlinearly Propagated Noise," *Journal of the Acoustical Society of America*, Vol. 121, No. 1, 2007, pp. EL1–EL7. https://doi.org/10.1121/1.2401193

[5] Swift, S. H., and Gee, K. L., "Examining the Use of a Time-Varying Loudness Algorithm for Quantifying Characteristics of Nonlinearly Propagated Noise (L)," *Journal of the Acoustical Society of America*, Vol. 129, No. 5, 2011, pp. 2753–2756. https://doi.org/10.1121/1.3569710

[6] Gee, K. L., Neilsen, T. B., Wall, A. T., Downing, J. M., James, M. M., and McKinley, R. L., "Propagation of Crackle-Containing Jet Noise from High-Performance Engines," *Noise Control Engineering Journal*, Vol. 64, No. 1, 2015, pp. 1–12. https://doi.org/10.3397/1/376354

[7] Blackstock, D. T., "Once Nonlinear, Always Nonlinear," *AIP Conference Proceedings*, Vol. 838, 2006, pp. 601–606.

[8] Mora, P., Heeb, N., Kastner, J., Gutmark, E. J., and Kailasanath, K., "Effect of Scale on the Far-Field Pressure Skewness and Kurtosis of Heated Supersonic Jets," AIAA Paper 2013-0616, 2013.

[9] Pernet, D. F., and Payne, R. C., "Non-Linear Propagation of Signals in Airs," *Journal of Sound and Vibration*, Vol. 17, No. 3, 1971, pp. 383–396. https://doi.org/10.1016/0022-460X(71)90650-X

[10] Morfey, C. L., and Howell, G. P., "Nonlinear Propagation of Aircraft Noise in the Atmosphere," *AIAA Journal*, Vol. 19, No. 8, 1981, pp. 986–992. https://doi.org/10.2514/3.51026

[11] Blackstock, D. T., "Nonlinear Propagation of Jet Noise," *Third Interagency Symposium on University Research in Transportation Noise*, U.S. Dept. of Transportation, Univ. of Utah, Salt Lake City, UT, 1975, pp. 389–397.

[12] Gurbatov, S. N., and Rudenko, O. V., "Statistical Phenomena," *Nonlinear Acoustics*, edited by M. F. Hamilton, and D. T. Blackstock, Academic Press, San Diego, CA, pp. 377–398.

[13] Rudenko, O. V., Gurbatov, S. N., and Demin, I. Y., "Absorption of Intense Regular and Noise Waves in Relaxing Media," *Acoustical Physics*, Vol. 60, No. 5, 2014, pp. 499–505. https://doi.org/10.1134/S106377101405011X

[14] Ffowcs-Williams, J. E. S., and Virchis, V. J., " 'Crackle': An Annoying Component of Jet Noise," *Journal of Fluid Mechanics*, Vol. 71, No. 2, 1975, pp. 251–271. https://doi.org/10.1017/S0022112075002558

[15] Muhlestein, M. B., Gee, K. L., Neilsen, T. B., and Thomas, D. C., "Evolution of the Average Steepening Factor for Nonlinearly Propagating Waves," *Journal of the Acoustical Society of America*, Vol. 137, No. 2, 2015, pp. 640–650. https://doi.org/10.1121/1.4906584

[16] Reichman, B. O., Muhlestein, M. B., Gee, K. L., Neilsen, T. B., and Thomas, D. C., "Evolution of the Derivative Skewness for Nonlinearly Propagating Waves," *Journal of the Acoustical Society of America*, Vol. 139, No. 3, 2016, pp. 1390–1403. https://doi.org/10.1121/1.4944036

[17] McInerny, S. A., "Launch Vehicle Acoustics. II—Statistics of the Time Domain Data," *Journal of Aircraft*, Vol. 33, No. 3, 1996, pp. 518–523. https://doi.org/10.2514/3.46975

[18] Gee, K. L., Neilsen, T. B., and Atchley, A. A., "Skewness and Shock Formation in Laboratory-Scale Supersonic Jet Data," *Journal of the Acoustical Society of America*, Vol. 133, No. 6, 2013, pp. EL491–EL497. https://doi.org/10.1121/1.4807307

[19] Fiévet, R., Tinney, C. E., Baars, W. J., and Hamilton, M. F., "Coalescence in the Sound Field of a Laboratory-Scale Supersonic Jet," *AIAA Journal*, Vol. 54, No. 1, 2015, pp. 1–12. https://doi.org/10.2514/1.J054252

[20] Baars, W., Tinney, C., Wochner, M., and Hamilton, M., "On Cumulative Nonlinear Acoustic Waveform Distortions from High-Speed Jets," *Journal of Fluid Mechanics*, Vol. 749, 2014, pp. 331–366. https://doi.org/10.1017/jfm.2014.228

[21] Reichman, B. O., Gee, K. L., Neilsen, T. B., Swift, S. H., and Wall, A. T., "Acoustic Shock Formation in Noise Propagation During Ground Run-Up Operations of Military Aircraft," AIAA Paper 2017-4043, 2017.

[22] Gee, K. L., Downing, J. M., James, M. M., McKinley, R. C., McKinley, R. L., Neilsen, T. B., and Wall, A. T., "Nonlinear Evolution of Noise from a Military Jet Aircraft During Ground Run-Up," AIAA Paper 2012-2258, 2012.

[23] Gee, K. L., Neilsen, T. B., Thomas, D. C., Reichman, B. O., Muhlestein, M., Downing, J. M., James, M. M., and McKinley, R. L., "Comparison of Two Time-Domain Measures of Nonlinearity in Near-Field Propagation of High-Power Jet Noise," *20th AIAA/CEAS Aeroacoustics Conference*, AIAA Paper 2014-3199, 2014.

[24] "Acoustics—Description, Measurement and Assessment of Environmental Noise—Part 1: Basic Quantities and Assessment Procedures," ISO Vol. 1996-1:2016, 2016.

[25] Gee, K. L., Atchley, A. A., Falco, L. E., and Shepherd, M. R., "Nonlinearity Analysis of Model-Scale Jet Noise," *19th International Symposium on Nonlinear Acoustics*, Vol. 1474, AIP Publishing, Tokyo, 2012, pp. 307–310.

[26] Petitjean, B. P., Viswanathan, K., and McLaughlin, D. K., "Acoustic Pressure Waveforms Measured in High Speed Jet Noise Experiencing Nonlinear Propagation," *International Journal of Aeroacoustics*, Vol. 5, No. 2, 2006, pp. 193–215. https://doi.org/10.1260/147547206777629835

[27] Gee, K. L., Sparrow, V. W., James, M. M., Downing, J. M., Hobbs, C. M., Gabrielson, T. B., and Atchley, A. A., "The Role of Nonlinear Effects in the Propagation of Noise from High-Power Jet Aircraft," *Journal of the Acoustical Society of America*, Vol. 123, No. 6, 2008, pp. 4082–4093. https://doi.org/10.1121/1.2903871

[28] McInerny, S. A., and Ölçmen, S. M., "High Intensity Rocket Noise: Nonlinear Propagation, Atmospheric Absorption, and Characterization," *Journal of the Acoustical Society of America*, Vol. 117, No. 2, 2005, 578–591. https://doi.org/10.1121/1.1841711

[29] Muhlestein, M. B., "Analyses of Nonlinearity Measures in High-Amplitude Sound Propagation," Master's Thesis, Physics and Astronomy, Brigham Young Univ., Provo, UT, 2013.

[30] James, M. M., Salton, A. R., Downing, J. M., Gee, K. L., Neilsen, T. B., Reichman, B. O., McKinley, R. L., Wall, A. T., and Gallagher, H. L., "Acoustic Emissions from F-35 Aircraft During Ground Run-Up," AIAA Paper 2015-2375, 2015.

C. Bailly
Associate Editor